Electronic Supplementary Material (ESI) for ChemComm.
This journal is © The Royal Society of Chemistry 2023

Supplementary Information for

Revealing the Origin of Activity in Phthalocyanine-Based Dual-Metal Sites Towards Electrochemical Nitric Oxide Reduction

Xiaorong Zhu, [†*] Xiaolei Yuan, [†] Yijin Wang, [†] Ming Ge, [†*] Yanfeng Tang[†*]

[†] School of Chemistry and Chemical Engineering, Nantong University, Nantong 226019, China.

*To whom correspondence should be addressed. Email:xiaorongzhu@ntu.edu.cn (XZ) and tangyf@ntu.edu.cn (YT)

Spin-polarized DFT calculations are performed using the Vienna ab initio simulation package (VASP)[1-2].The exchange-correlation energy is described using the Perdew-Burke-Ernzerhof (PBE) functional within the generalized gradient approximation (GGA)[3-4]. A kinetic energy cutoff of 500 eV is adopted, whereas the core electrons are modeled by projector augmented wave (PAW) pseudo potentials[5]. The convergence criteria are set at 10^{-5} eV for total energy and 0.02 eV $Å^{-1}$ for force. In this work, ten transition metal bi-atom pairs are decorated in phthalocyanine caves. The Brillouin zone is sampled using a $3\times3\times1$ Monkhorst-Pack k-point grid for structural optimizations, while a denser mesh of $9\times9\times1$ is used for electronic structure computations. A vacuum space of $\approx$15 Å is added to eliminate interactions between two adjacent periodic images. vdW interactions between catalysts and reaction intermediates are described using DFT + D3[6].

The computational hydrogenation electrode (CHE) model developed by Nørskov et al.[7] is used to study the free energy profile of NORR. The Gibbs free energy change for each elementary step is calculated using the following equation:

$$\Delta G = \Delta E + \Delta E_{ZPE} - T\Delta S + \Delta G_U + \Delta G_{pH}$$

where the ΔE is obtained from the DFT calculations, ΔE_{ZPE} is the zero-point energy change between the reactants and products. T is the temperature (298.15 K), and the ΔS represents the change in entropy of products and reactants. $\Delta G_{pH} = -k_B T \ln 10 \times pH$, k_B is the Boltzmann constant and the pH was set as zero. ΔG_U is the free energy change of the electrode potential. Bader charge analysis evaluates charge transfer between bi-atom pairs and substrate N coordinates.

The stability of TM_2-Pc is evaluated by the formation energy and the dissolution energy[8], represented as:

$$E_{formation} = \frac{1}{2} \times (E_{TM2-Pc} - E_{Pc} - 2E_{TM})$$

$$U_{diss} = U^0_{diss}(TM, bulk) - E_{formation} / eNe$$

Where the $E_{TM2-Pc}, E_{Pc}, E_{TM}$ represent the total energies of BACs (TM_2-Pc，O-TM_2-Pc), DACs without TM atoms, and metal atoms in the most stable bulk structure, respectively. $U^0_{diss}(TM, bulk)$ and the Ne represent the represent the standard dissolution potential of the bulk metal and the number of electrons involved in the dissolution, respectively.

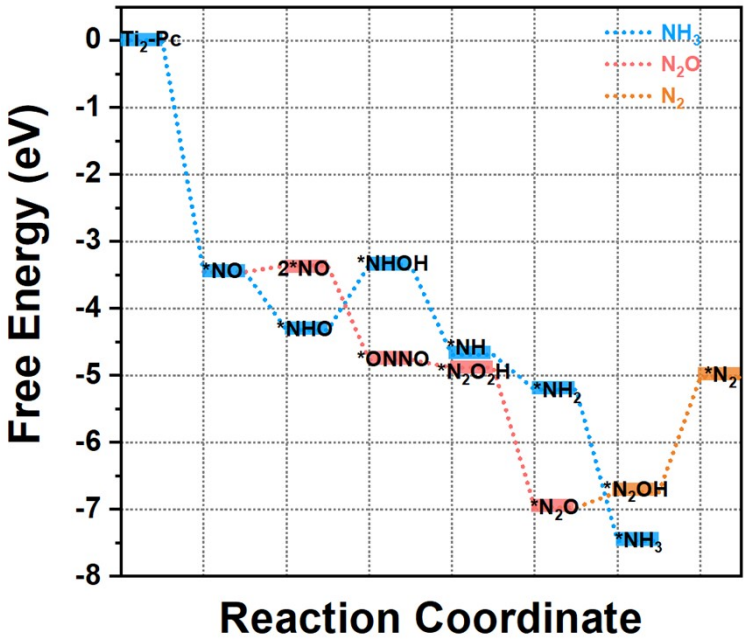

Fig. S1. The free energy diagram of NO reduction (toward NH_3, N_2O, N_2 formation) on Ti_2-Pc

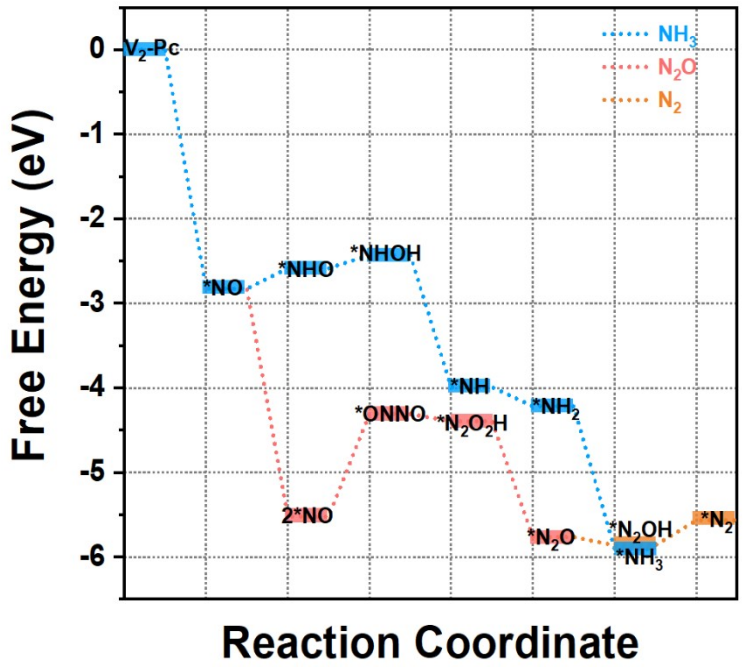

Fig. S2. The free energy diagram of NO reduction (toward NH_3, N_2O, N_2 formation) on V_2-Pc

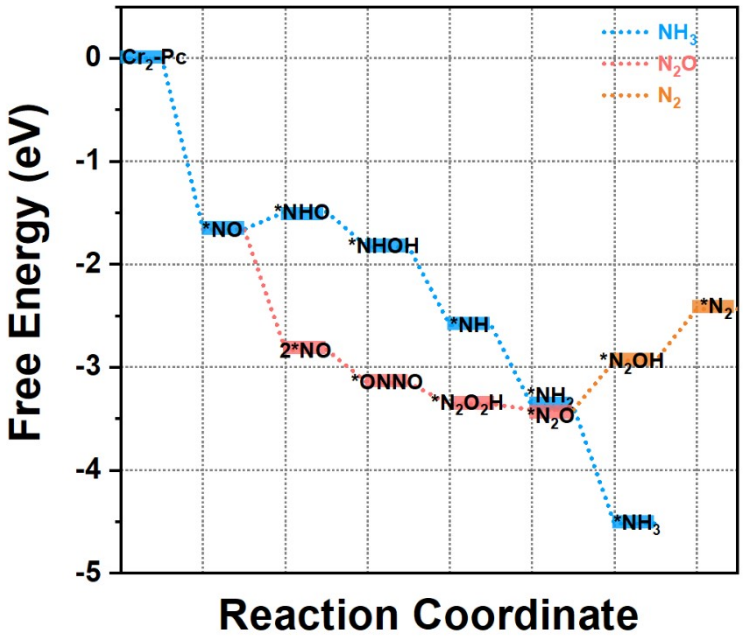

Fig. S3. The free energy diagram of NO reduction (toward NH_3, N_2O, N_2 formation) on Cr_2-Pc

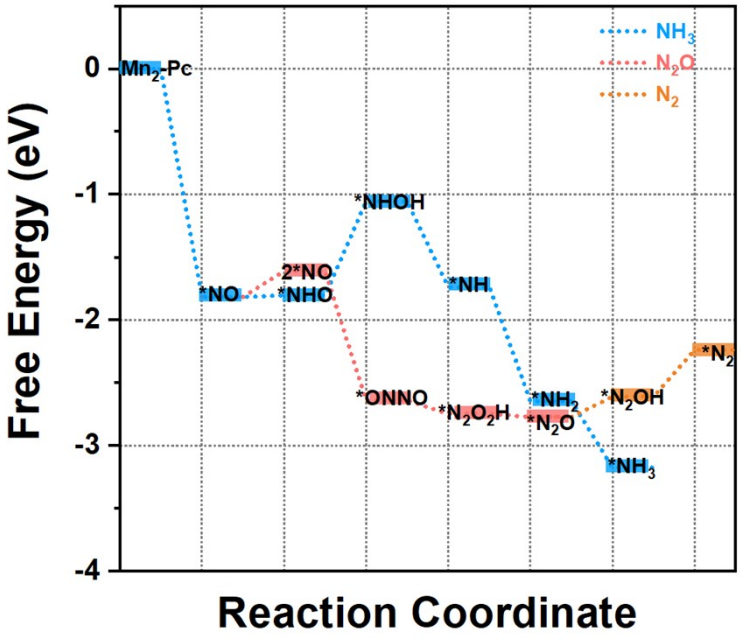

Fig. S4. The free energy diagram of NO reduction (toward NH_3, N_2O, N_2 formation) on Mn_2-Pc

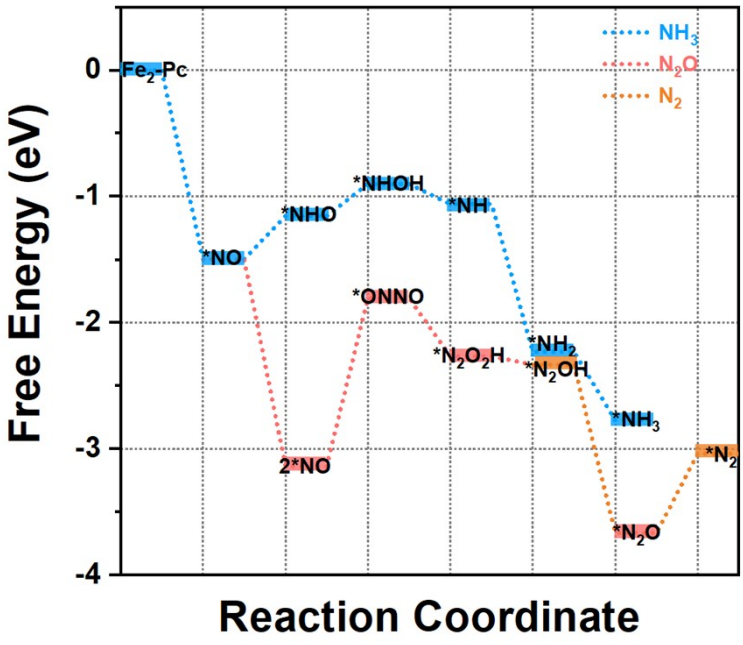

Fig. S5. The free energy diagram of NO reduction (toward NH_3, N_2O, N_2 formation) on Fe_2-Pc

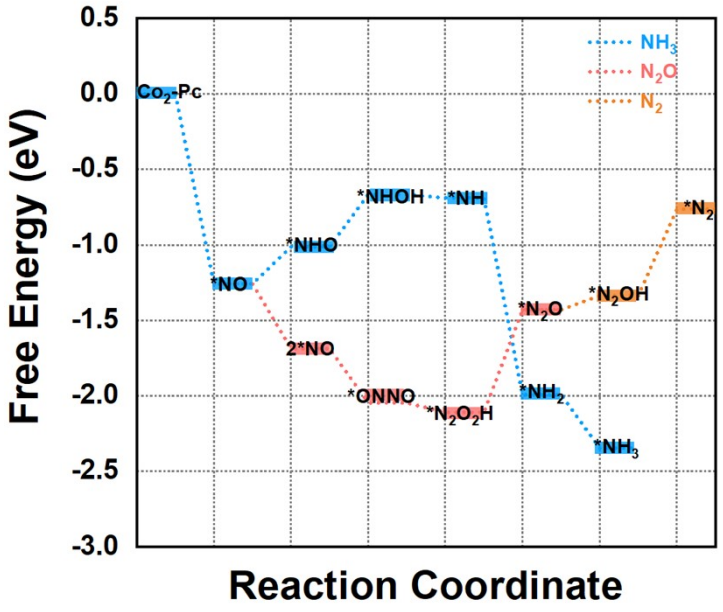

Fig. S6. The free energy diagram of NO reduction (toward NH_3, N_2O, N_2 formation) on Co_2-Pc

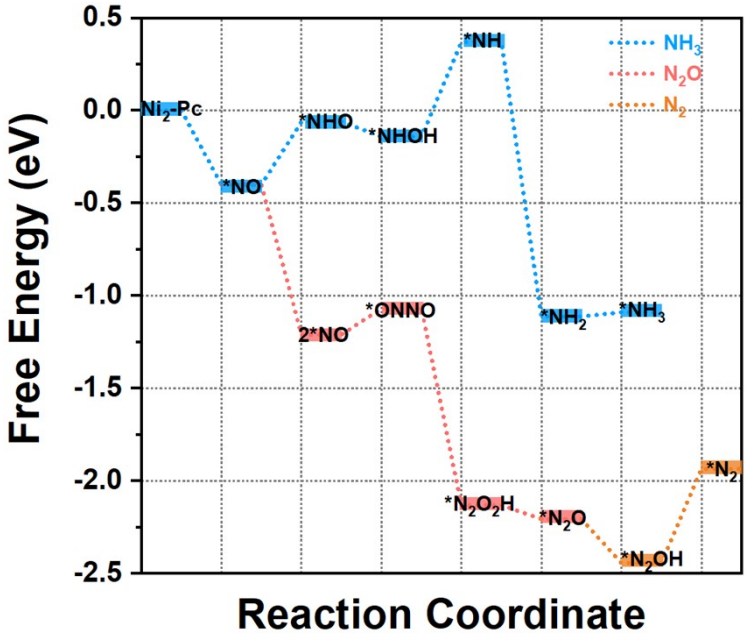

Fig. 7. The free energy diagram of NO reduction (toward NH_3, N_2O, N_2 formation) on Ni_2-Pc

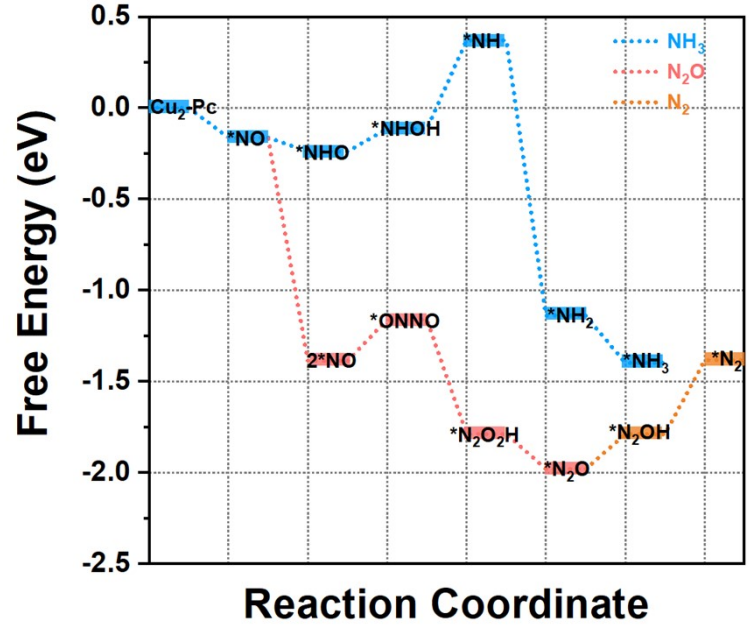

Fig. S8. The free energy diagram of NO reduction (toward NH_3, N_2O, N_2 formation) on Cu_2-Pc

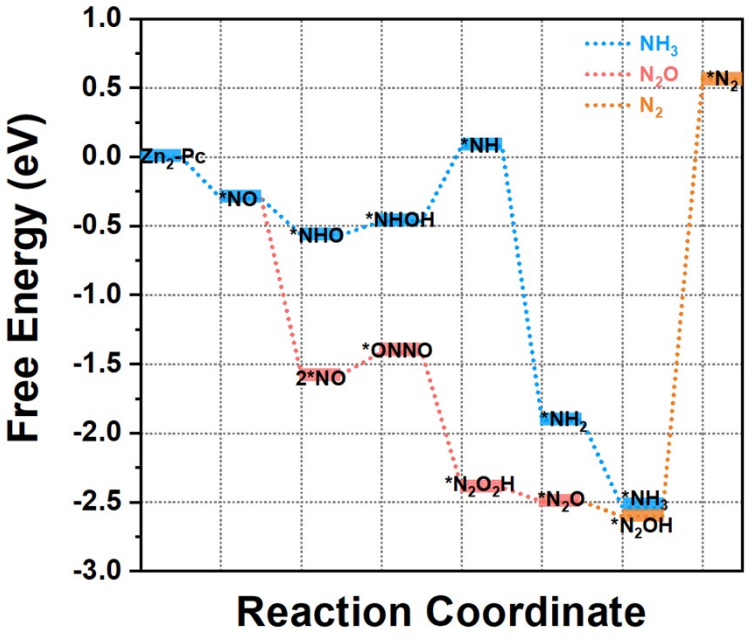

Fig. S9. The free energy diagram of NO reduction (toward NH_3, N_2O, N_2 formation) on Zn_2-Pc

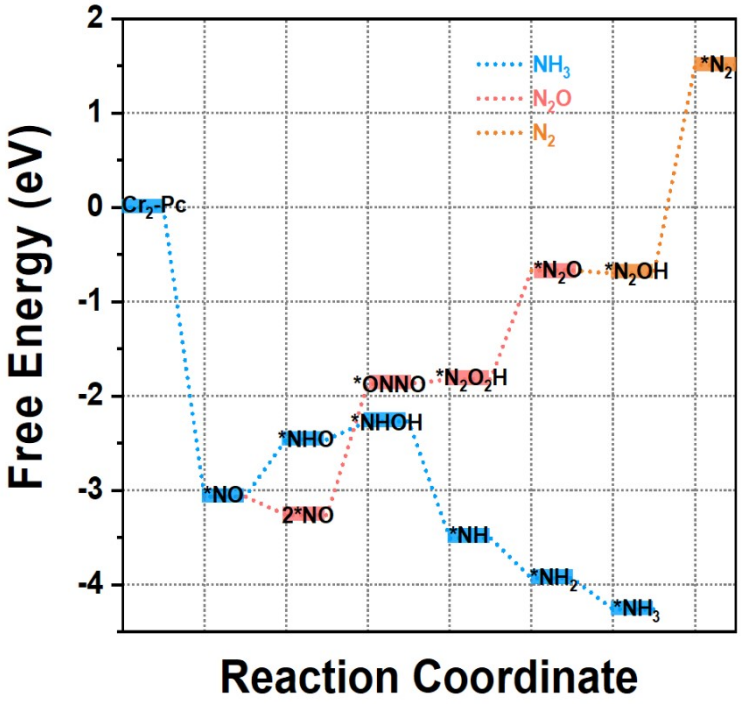

Fig. S10. The free energy diagram of NO reduction (toward NH_3, N_2O, N_2 formation) on O-ligand modified Cr_2-Pc

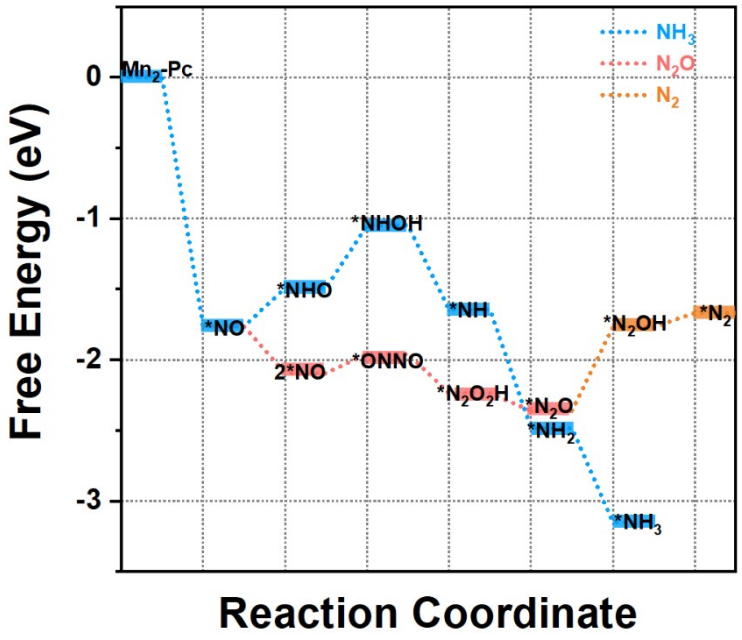

Fig. S11. The free energy diagram of NO reduction (toward NH_3, N_2O, N_2 formation) on O-ligand modified Mn_2-Pc

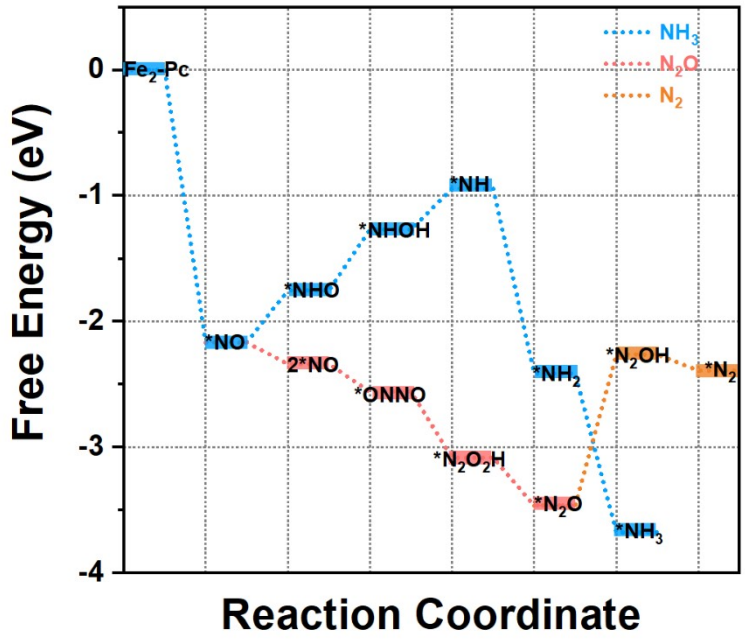

Fig. S12. The free energy diagram of NO reduction (toward NH_3, N_2O, N_2 formation) on O-ligand modified Fe_2-Pc

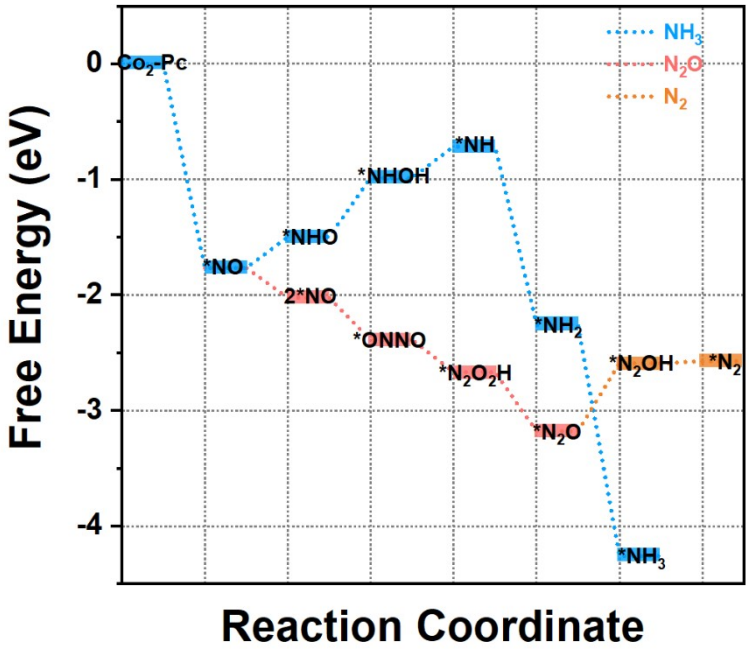

Fig. S13. The free energy diagram of NO reduction (toward NH_3, N_2O, N_2 formation) on O-ligand modified Co_2-Pc

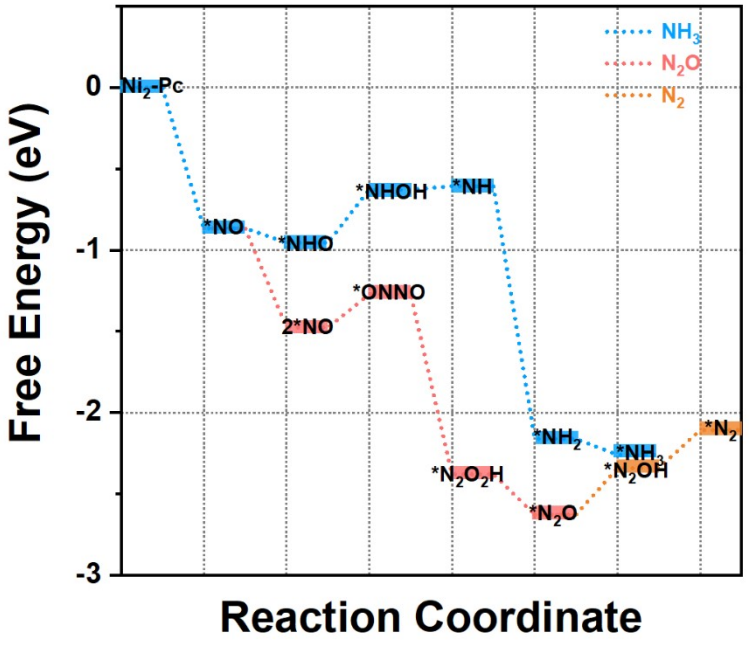

Fig. S14. The free energy diagram of NO reduction (toward NH_3, N_2O, N_2 formation) on O-ligand modified Ni_2-Pc

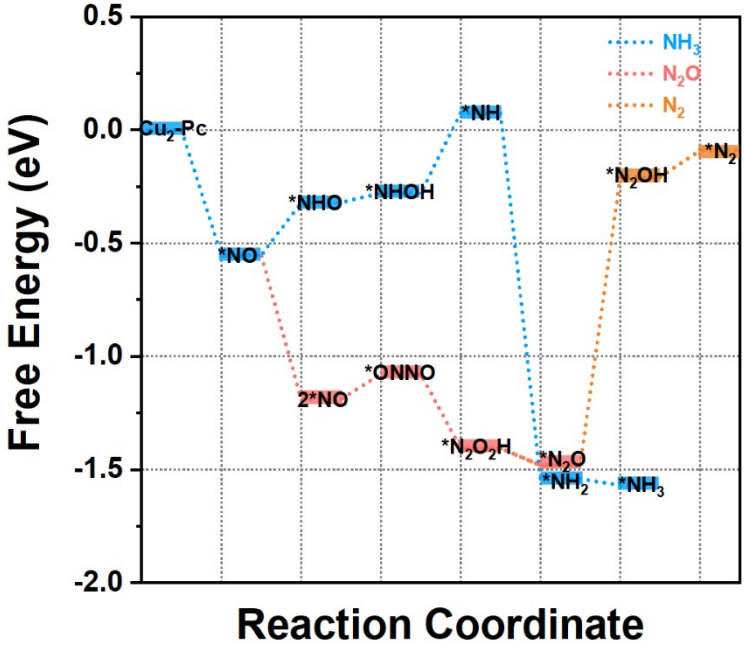

Fig. S15. The free energy diagram of NO reduction (toward NH_3, N_2O, N_2 formation) on O-ligand modified Cu_2-Pc

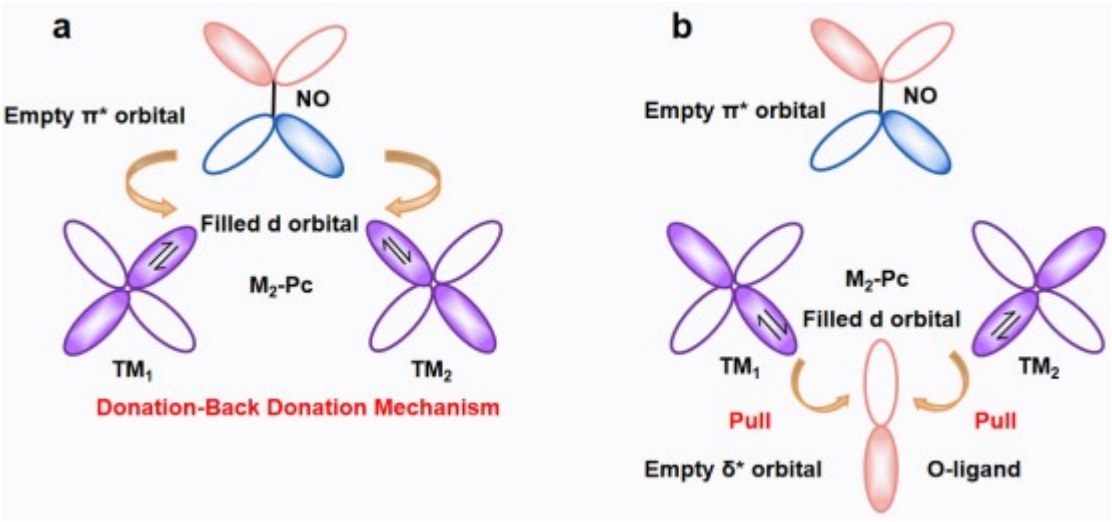

Figure S16 The schematic diagram illustrates the donation-back donation mechanism of NO on TM_2-Pc surfaces and the pulling effect diagram after the introduction of O axial ligand.

Table S1 The formation energy and the dissolution energy of pristine TM_2-Pc.

	Surface	Substrate	Metal	E_f	U_{diss}	U^0_{diss}	Ne
Co_2-Pc	-413.71	-390.59	-27.88	-4.59	1.01	-0.28	2.00
Cr_2-Pc	-419.54	-390.55	-36.38	-5.40	0.90	-0.91	2.00
Cu_2-Pc	-404.41	-389.95	-14.88	-3.51	1.05	0.34	2.00
Fe_2-Pc	-416.57	-392.73	-32.31	-3.84	0.74	-0.45	2.00
Mn_2-Pc	-418.88	-390.61	-35.60	-5.24	0.71	-1.19	2.00
Ni_2-Pc	-410.95	-390.61	-21.80	-4.72	1.05	-0.26	2.00
Sc_2-Pc	-413.96	-389.92	-24.60	-5.87	-0.06	-2.08	3.00
Ti_2-Pc	-416.69	-390.33	-30.82	-5.48	0.55	-1.63	2.00
V_2-Pc	-418.51	-390.53	-34.74	-5.31	0.74	-1.18	2.00
Zn_2-Pc	-399.67	-390.38	-2.19	-4.10	0.64	-0.76	2.00

Table S2 The formation energy and the dissolution energy of pristine O-TM_2-Pc.

	Surface	**Substrate**	**Metal**	**E_f**	**U_{diss}**	**U^0_{diss}**	**Ne**
O-Co_2-Pc	-417.45	-391.90	-27.88	-5.80	1.31	-0.28	2.00
O-Cr_2-Pc	-427.10	-391.87	-36.38	-8.52	1.67	-0.91	2.00
O-Cu_2-Pc	-406.86	-391.29	-14.88	-4.07	1.19	0.34	2.00
O-Fe_2-Pc	-421.22	-392.17	-32.31	-6.44	1.39	-0.45	2.00
O-Mn_2-Pc	-424.73	-391.99	-35.60	-7.47	1.27	-1.19	2.00
O-Ni_2-Pc	-413.64	-391.96	-21.80	-5.39	1.22	-0.26	2.00
O-Ti_2-Pc	-426.58	-391.08	-30.82	1.78	-1.26	-1.63	2.00
O-V_2-Pc	-427.28	-391.34	-34.74	8.69	-2.76	-1.18	2.00
O-Zn_2-Pc	-403.53	-391.67	-2.19	0.55	-0.52	-0.76	2.00

Table S3 The bader charge and d band centers of transition metal pairs in pristine and axial O ligand modified TM_2-Pc.

	Bader Charge (TM_2-Pc)	**d Band Center (TM_2-Pc)**	**Bader Charge (O-TM_2-Pc)**	**d Band Center (O-TM_2-Pc)**
Co	-0.90	-3.74	-1.17	-3.55
Cr	-1.32	-3.46	-1.32	-3.46
Cu	-0.96	-3.92	-0.96	-3.92
Fe	-1.05	-3.78	-1.05	-3.78
Mn	-1.21	-3.62	-1.21	-3.62
Ni	-0.92	-3.46	-0.92	-3.46
Ti	-1.59	-3.46	-1.59	-3.46
V	-1.40	-3.27	-1.40	-3.27
Zn	-1.16	-4.09	-1.16	-4.09

Table S4 The spin populations of transition metal pairs in pristine and axial O ligand modified V_2-Pc，Cr_2-Pc，Fe_2-Pc.

	Spin Populations (TM_2-Pc)	**Spin Populations (O-TM_2-Pc)**
V	3.71	0.00
Cr	6.00	0.38
Fe	2.08	0.00

Reference

1 G. Kresse, J. Furthmüller, Phys. Rev. B, 1996, **54**, 11169−11186.

2 G. Kresse, J. Hafner, Phys. Rev. B, 1993, **47**, 558−561.

3 J. P. Perdew, K. Burke, M. Ernzerhof, Phys. Rev. Lett., 1996, **77**, 3865−3868.

4 P. E. Blöchl, Phys. Rev. B, 1994, **50**, 17953−17979.

5 G. Kresse, D. Joubert, Phys. Rev. B: Condens. Matter Mater. Phys., 1999, **59**, 1758.

6 S. Grimme, J. Antony, S. Ehrlich, H. Krieg, J. Chem. Phys. 2010, **132**, 154104.

7 J. K. Nørskov, J. Rossmeisl, A. Logadottir, L. Lindqvist, J. R. Kitchin, T. Bligaard, H. Jónsson, J. Phys. Chem. B, 2004, **108**, 17886−17892.

8 J. Greeley, J. K. Nørskov, Electrochim. Acta, 2007, **52**, 5829−5836.